JOURNAL OF PROPULSION AND POWER
Vol. 10, No. 2, March–April 1994

Demonstration and Evaluation of Carbon-Carbon Ion Optics

D. E. Hedges* and J. S. Meserole†
Boeing Defense and Space Group, Seattle, Washington 98124

The principal life-limiting component of ion thrusters is the ion optics set used to electrostatically accelerate ionized propellant from the thruster's discharge chamber. An ion optics set consists of two or three thin, closely spaced, multiaperture grids, usually made of molybdenum. Grid lifetime is limited by sputter erosion from ion impingement. Data in the literature show that carbon is about five times more resistant to sputter erosion than molybdenum. Carbon in the form of graphite is used for laboratory ion optics, but graphite is too fragile for spacecraft use. Use of carbon-carbon composites may enable fabrication of rugged, thermomechanically stable optics with greater lifetime than molybdenum. This article describes a laboratory demonstration of a flat, two-grid, 10-cm-diam carbon-carbon ion optics set, with an evaluation of selected performance characteristics relative to a molybdenum optics set of roughly similar geometry. The carbon-carbon optics delivered stable operation at a cold grid gap of 0.2 mm, an average current density of 2.2 mA/cm², and an inferred voltage gradient of 6400 V/mm. Differences observed in the maximum perveance condition, the electron backstreaming limit, and the defocusing limit between the two optics sets were consistent with the known geometrical differences.

Nomenclature

A = screen grid open area
d_a = accelerator grid hole diameter
d_s = screen grid hole diameter
J_b = measured beam current
J_c = space-charge-limited (Child's law) current
l_e = effective acceleration length
l_g = grid-to-grid gap
$\mathcal{P}$ = perveance, $(J_b/V_t)^{3/2}$
q/M = ion charge-to-mass ratio
R = net-to-total voltage ratio, V_b/V_t
t_a = accelerator grid thickness
t_s = screen grid thickness
V_a = accelerator grid voltage
V_b = beam (also net accelerating) voltage
V_d = discharge voltage
V_t = total acceleration voltage
ε_0 = permittivity of free space
η_u = propellant utilization efficiency

Introduction

ION propulsion systems offer substantial improvements in spacecraft payload mass fraction when compared to conventional chemical propulsion systems for missions with large velocity change requirements, such as for solar system exploration and for satellite orbit maneuvering. This mass fraction advantage results from the higher propellant exhaust velocities attainable with electrostatic acceleration. However, the power to accelerate the propellant from an ion thruster must come from a power supply carried with the spacecraft rather than from the stored chemical energy of the propellants. Since available power is limited, the rate at which propellant is accelerated to these high exhaust velocities is limited. As a result, thrust levels for ion propulsion systems are at least two orders of magnitude lower than for chemical propulsion systems. Therefore, long transfer times are required and long-term reliability (on the order of 10,000 h) must be demonstrated before ion propulsion technology is applied to future spacecraft.

One component that limits ion thruster reliability is the ion optics set (consisting of a screen grid and an accelerator grid for a two-grid set) that extracts ionized propellant from the thruster's discharge chamber. In a recent study by Patterson[1] of lifetime expectations for a 30-cm xenon ion thruster operating at specific impulses ranging from 1000 to 2500 s, the accelerator grid was the minimum-life component for approximately 80% of the thruster operational envelope, and for all conditions for which lifetime was less than 10,000 h.

Role of Ion Optics in Lifetime and Performance

Effect on Lifetime

Optics lifetime is limited by erosion caused by ion impingement. Direct ion impingement occurs when ions are not properly focused as they accelerate through the grids. Charge exchange ion impingement occurs when fast ions interact with slow neutral atoms to produce slow ions that are attracted to the negative potential of the accelerator grid. Even with properly focused optics, charge exchange ions will steadily erode the accelerator grid, particularly on its downstream side.

One way to reduce the rate of erosion due to charge exchange ions is to lower the beam current density, but this approach limits thruster performance. Another option is to use a material that has a high resistance to sputter erosion. Conventional grids use molybdenum, but data presented by Wehner[2] and others show that the sputtering yield (in atoms per ion) for 500-eV xenon ions impacting carbon is five times lower than for the same ions impacting molybdenum.

Effect on Performance

Heating from the discharge chamber plasma will cause flat metal grids to warp. Therefore, the grids must be hydroformed into a dished or convex shape to control warpage and to minimize changes in spacing as temperature increases. The dished shape makes accurate grid alignment more difficult. In addition, as grid size increases, it becomes more difficult to maintain close, uniform spacing, which is an important factor influencing thruster performance.

Close spacing is necessary to maximize the achievable thrust-to-weight ratio. For a given electric field strength between grids, there is a limit to how many ions can reside between the grids without their collective space charge shielding the

Received Oct. 30, 1992; revision received June 7, 1993; accepted for publication June 24, 1993.

*Senior Specialist Engineer, Engineering Division, P.O. Box 3999, M/S 82-23. Senior Member AIAA.
†Principal Engineer, Engineering Division, P.O. Box 3999, M/S 82-23. Senior Member AIAA.

Table 1 Ion optics geometry

	Molybdenum			Carbon-carbon		
Grid shape	Circular, dished in 7.2 mm			Circular, flat		
Beam diameter, cm	9.6			9.6		
Hole quantity	1614			1615		
Hole spacing, mm	2.29			2.29		
Hole profile	Cupped			Tapered 6 deg		
Screen grid open area fraction	0.63			0.59		
Accelerator grid open area fraction	0.23			0.21		
t_s, mm	0.36			0.79		
t_a, mm	0.38			0.89		
d_s, mm	1.90			1.83		
d_a, mm	1.14			1.09		
l_g, mm	0.6	0.7	0.9	0.2	0.3	0.5
l_e, mm	1.35	1.42	1.58	1.35	1.42	1.58

discharge plasma from the accelerator grid potential. As this maximum beam density is approached, the accelerator grid is less able to accelerate and focus the ionized propellant through the apertures in the grid, and some of the ions strike the accelerator grid. Closer grid spacing increases the electric field strength between the grids for a given applied voltage. This increases the beam density limit at which direct ion impingement occurs, and that in turn maximizes the achievable thrust-to-weight ratio.

Uniform spacing is necessary so that the entire grid area can operate at its design point. Nonuniformities can cause local areas that are susceptible to arcing or to increased erosion from either direct ion impingement or charge exchange ions. These nonuniformities will force operation at an average beam density that is lower than the design point.

If a grid material were used that had a very low or slightly negative coefficient of thermal expansion, then dishing might be eliminated and closer, more uniform spacing may be achievable.

Carbon as an Alternate Ion Optics Material

In 1963, flat graphite grids were tested as a potential solution to grid warpage from thermal distortion.[3] The graphite grids gave performance results comparable to those of a geometrically similar molybdenum set, but the brittle nature of the material was cited as a serious drawback.

Today, carbon-carbon composites made of carbon fiber imbedded in a carbon matrix provide a pure-carbon material that is exceptionally strong and rigid. These materials, moreover, can be made to have a near-zero or slightly negative coefficient of thermal expansion (CTE) over the range of operating temperatures of ion thrusters.

Carbon-carbon offers the following potential advantages over molybdenum: 1) higher erosion resistance, 2) a flat geometry that is easier to align, and 3) closer spacing and/or larger grid area due to improved thermomechanical stability. Thus, carbon-carbon ion optics may improve both the life and the performance of ion thrusters.

Six carbon-carbon panels were acquired by the present authors in 1989 to evaluate carbon-carbon's suitability as a material for ion thruster grids. As part of an initial evaluation, measurements were made of the CTE of the panels, and a laser was used to cut sample holes of selected sizes and spacings. CTE measurements ranged from -2.0×10^{-6}/K at 295 K to about $+1.0 \times 10^{-6}$/K at 673 K. The laser machining process gave clean, repeatable hole patterns without any laser-induced warpage in the panels. Subsequently, 10-cm-diam screen and accelerator grids were manufactured from two of the panels and were tested on a thruster.

Current Effort

This article describes the fabrication and testing of a flat 10-cm carbon-carbon ion optics set to demonstrate its operation and evaluate some of its performance characteristics. The test was intended primarily to ensure that carbon-carbon did not give rise to unusual or unexpected operational behavior relative to molybdenum. Other objectives were to determine if carbon-carbon grids could give stable thruster operation with narrow grid spacing (i.e., less than 0.5 mm) and to investigate carbon-carbon's ability to support large voltage gradients (above 5000 V/mm). As part of the performance evaluation, the maximum perveance condition, electron backstreaming limit, and defocusing limit for the carbon-carbon optics set were determined. To provide a reference for these measurements, the performance evaluation was repeated with a conventional molybdenum optics set of roughly similar geometry.

Related Work

In related work, Monheiser and Wilbur[4] conducted comparative erosion tests of molybdenum and graphite grids. Erosion depth profiles using a profilometer showed that the molybdenum grids eroded several times faster than the graphite grids. Garner and Brophy[5] fabricated carbon-carbon panels for ion optics applications, and conducted CTE measurements and erosion tests of the panels. The CTE's of the panels were negative up to approximately 900 K. In erosion rate tests conducted in the discharge chamber of an ion engine operated on argon, they found that badges of carbon-carbon eroded at a rate approximately 25% less than badges of molybdenum. In addition, they reported promising results using electrostatic discharge machining to produce a set of three 15-cm-diam carbon-carbon grid plates with a representative array of over 500 holes in a 4- × 5-cm region at the center of each plate.

Ion Optics Description

Conventional Molybdenum Grids

The molybdenum grids used as a basis for this evaluation were a pair of 10-cm-diam, dished, circular grids (along with a molybdenum grid mount) that had previously been obtained. The grid geometry is described further in Table 1. The grid holes were etched by chemical milling. The screen grid holes were etched equally from each side, whereas the accelerator grid holes were etched primarily from the downstream side, producing cupped-hole cross sections as shown in Fig. 1a. When installed on the ion source, the optics dished into the ion source discharge chamber.

Carbon-Carbon Grids

A pair of 10-cm-diam, flat, circular grids were fabricated from two 14-cm-square by 0.8–0.9-mm-thick carbon-carbon panels. Their geometry is also described in Table 1. The panels are constructed of a pitch-based carbon fiber with a modulus of 7.2×10^{11} Pa and a diameter of 10 μm. The fibers are woven into fabric 0.28-mm thick using a 5-harness satin weave.

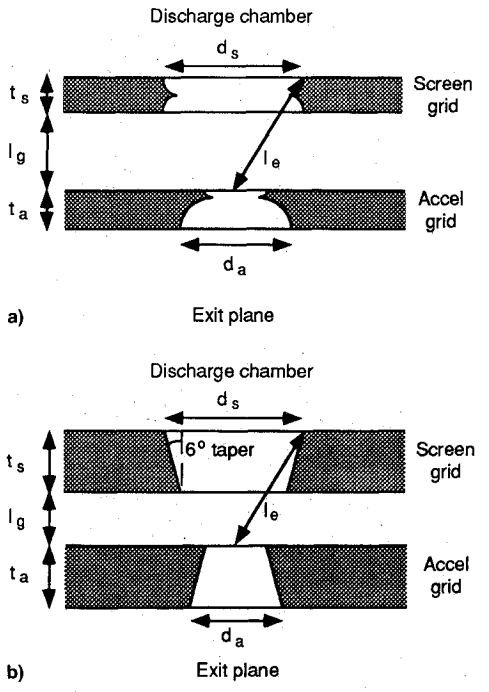

Fig. 1 Grid hole profiles for a) molybdenum grids and b) carbon-carbon grids.

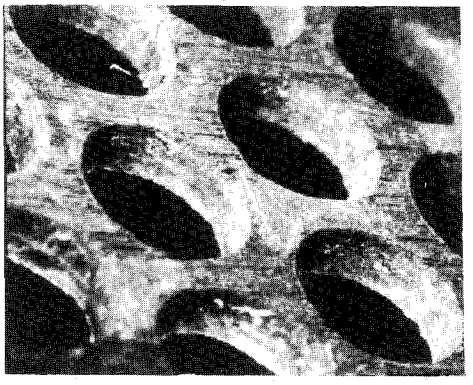

Fig. 2 Laser-machined holes in a carbon-carbon test coupon.

Each panel consists of three plies of fabric laid up in a [0,45,0] orientation and densified with a carbon matrix using a chemical vapor infiltration process. The panels were available without a special order, which enabled expeditious and cost-effective proof-of-concept tests, although with relatively thick grids.

As delivered, the panels were slightly warped, with one corner approximately 1 mm above a flat surface when the opposing corner was restrained to the surface. However, by restraining two opposing corners, the panels easily snapped to a flat configuration.

The panels were machined to nearly the same geometry (in terms of hole quantity, diameter, and spacing) as the 10-cm molybdenum grids. This was done using a 1.5-kW CO_2 laser. The laser produced holes with a 6-deg taper as shown in Fig. 1b, with the larger diameter on the laser-entry side. Figure 2 is a close-up of a carbon-carbon test coupon that was laser-machined. It has 2.3-mm-diam holes on 3.0-mm centers. The appearance of the surface and hole finish are typical of the carbon-carbon grids used in this study.

No special surface preparation (either cleaning or smoothing) was done prior to grid testing. The laser machining process left a soot-like discoloration on the laser-entry side of each grid. The surface roughness due to the fiber weave was ± 0.05 mm as measured by a diamond-stylus profilometer. The fiber heights were consistent enough, however, that the grids were measured to be flat to within 0.025 mm when installed on the grid mount. The grid mount provided continuous support around the periphery of each grid. Flatness was measured by a depth micrometer referenced to a surface established above the grids by a set of precision parallel blocks. (The grids retained the warpage that the original panels had when unrestrained, but the grids easily conformed to a flat configuration when fastened down at two points or more points on their periphery.)

Test Apparatus

The optics tests were conducted using a commercially available 15-cm ion source with integral water cooling. An adapter was built to mask down the 15-cm source to 10 cm and to accept a separate molybdenum grid mount that was used for both the molybdenum and the carbon-carbon grids.

The ion source used tungsten filaments for both the cathode and neutralizer. The cathode and neutralizer were driven by variable alternating current sources (variacs). The cathode was isolated from its variac using an isolation transformer. The beam supply was rated at 3000 V and 1 A and was referenced to facility ground. The discharge supply floated at beam potential with its positive terminal connected to the positive terminal of the beam supply and its negative terminal connected to the midpoint of the secondary winding on the cathode isolation transformer. The discharge supply was rated at 200 V and 17 A. The accelerator supply was rated at 600 V and 1.5 A. Xenon was used as the propellant. The tests were conducted in a diffusion-pumped vacuum chamber, 0.9 m in diameter by 1.8 m in height, that maintained a background pressure of approximately 5×10^{-5} Torr during testing.

A digital data acquisition system measured beam voltage and current, accelerator grid voltage and current, discharge voltage and current, cathode filament current, neutralizer filament and emission current, and propellant flow. Vacuum chamber pressure was measured with an ion gauge.

Test Procedure

Voltage Standoff Capability

Voltage standoff tests were conducted before operating the grids on the thruster. Each optics set in turn was mounted to the molybdenum grid mount, gapped to 0.58 mm (0.23 in.), and then tested in both air and vacuum until voltage breakdown occurred. A high-voltage variable dc power supply was used with a 100-k-Ω power resistor in series to limit the current when arcing occurred. No measurements were made of grid deflection as a function of applied voltage, so calculations of the voltage gradient are based on the initial grid gap.

General Run Conditions

Prior to starting the thruster for each run, the chamber background pressure was recorded while xenon flowed at the desired rate. The thruster was then started and allowed to warm up for at least 30 min prior to data acquisition. For all runs, the initial run conditions were as follows:

1) η_u was set to approximately 75%, determined by the ratio of beam current to propellant flow rate. (Flow rate was converted to an equivalent current using 1 A = 13.95 standard cubic centimeters per minute for singly ionized atoms.)

2) V_d was set to 35 V, which was less than or equal to 10% of V_t. The total accelerating voltage is given by

$$V_t = V_b + |V_a| \tag{1}$$

3) R was set to 0.8, where

$$R = (V_b/V_t) \tag{2}$$

4) The total voltage was set high enough to preclude direct ion impingement (by choosing a V_t such that further increases

Table 2 Performance evaluation test matrix, repeated for each optics set

	l_e, mm				
	1.35		1.42	1.58	
Test condition	1	2	3	4	5
J_b, mA	80	100	120	140	160
Xe flow rate, sccm[a]	1.5	1.8	2.2	2.6	3.0
Determine	Procedure				
1) Maximum perveance condition	a) Start above impingement-limited V_t, with $R = 0.8$ b) Measure J_a vs V_b as V_b is decreased, with J_b and V_a fixed				
2) Electron backstreaming limit	a) Start above impingement-limited V_t, with $R = 0.8$ b) Decrease V_a at given J_b and fixed V_b until J_b increases				
3) Defocusing limit	a) Start above impingement-limited V_t, with $R = 0.8$ b) Measure J_a vs R at fixed V_t				

[a]Standard cubic centimeters per minute.

in V_t at a fixed R did not reduce accelerator grid impingement current).

Maximum Perveance Condition

Perveance expresses total current in terms of applied voltage[6]:

$$\mathcal{P} = (J_b/V_t^{3/2}) \tag{3}$$

For fixed J_b, the maximum perveance condition of an optics set occurs at the lowest V_t at which direct ion impingement of the accelerator grid does not occur. For each set of grids, accelerator grid impingement current was measured as a function of decreasing beam voltage to identify the onset of direct ion impingement. Measurements were made for each of five beam current levels from 80 to 160 mA, and for three effective acceleration lengths (defined below). Beam current was held constant by adjusting the discharge current as necessary in response to changes in the beam voltage. Accelerator grid voltage was fixed for each run.

For the idealized case where the ion optics are modeled as a plane diode that is operating at space-charge-limited (or Child's law) current,[6] the current is given by

$$J_c = \frac{4\varepsilon_0}{9} A \left(\frac{2q}{M}\right)^{1/2} \frac{V^{3/2}}{x^2} \tag{4}$$

where A is the area of the ion emitting surface, q/M is the charge-to-mass ratio of the current carrier, and x is the gap between the plane diode surfaces. This expression can be used to normalize the measured beam currents at the maximum perveance condition by replacing A with the open area of the screen grid, and by replacing x with the effective acceleration length.

For this study, the effective acceleration length was assumed to be

$$l_e = \sqrt{(l_g + t_s)^2 + (d_s/2)^2} \tag{5}$$

to account for the thickness of the screen grid[1] (Fig. 1). l_g (measured from the downstream edge of the screen grid to the upstream edge of the accelerator grid) for the carbon-carbon optics was smaller than for the molybdenum optics at each effective acceleration length to account for the greater thickness of the carbon-carbon screen grid.

Electron Backstreaming Limit

Electron backstreaming occurs when the accelerator grid voltage is no longer sufficient to shield external electrons from the positive potential of the discharge chamber. Electrons are then free to flow from the external environment into the discharge chamber.

After completing each run of data points for determining the maximum perveance condition, the run's initial conditions were re-established. Beam current was then measured as a function of decreasing accelerator grid voltage to identify the onset of electron backstreaming for each run condition. The accelerator grid voltage was slowly reduced as the analog current meter on the beam supply was monitored. As the accelerator grid voltage fell below the electron backstreaming limit, a rapid increase in current through the beam supply was observed. The accelerator grid voltage at which this occurred was recorded as the electron backstreaming limit.

Defocusing Limit

After completing each run of data points for determining the electron backstreaming limit, the run's initial conditions were again re-established. Accelerator grid impingement current was then measured as a function of R while holding total voltage constant. This determined the minimum R that could be achieved without incurring direct ion impingement. For the selected total voltage, R was adjusted down from an initial value of 0.8 by first decreasing the beam (or net accelerating) voltage, and then increasing the accelerator grid voltage by the same amount to hold the total voltage constant. At each step, accelerator grid impingement current was recorded. As the defocusing limit was approached, the accelerator grid impingement current increased from the background level. The value of R at which the accelerator grid current first increased above the background level was identified as the defocusing limit for each run condition.

Test Matrix

The test matrix is shown in Table 2. It was designed to gather data on the maximum perveance condition, electron backstreaming limit, and defocusing limit for each optics set over the range of beam currents achievable with the ion source and to gather data at three effective acceleration lengths.

The effective acceleration lengths were chosen to be comparable with those used in prior work.[7] For the molybdenum grids, this gave grid-to-grid gaps of 0.6, 0.7, and 0.9 mm. To maintain the same effective acceleration lengths for the thicker carbon-carbon grids, closer grid-to-grid gaps of 0.2, 0.3, and 0.5 mm were used. No capability existed to monitor or adjust grid spacing as the grids heated up during testing. Therefore, all grid gaps and effective acceleration lengths reported are based on cold (room temperature) measurements. Likewise, all voltage gradient estimates are based on the cold grid gap.

Average beam current densities ranged from 1.1 mA/cm^2 at $J_b = 80$ mA to 2.2 mA/cm^2 at $J_b = 160$ mA, based on a 9.6-cm beam diameter. The flatness parameter (the ratio of the average current density to the peak current density) of the ion source is better than 0.5, based on measurements from the manufacturer. So with the source masked from 15 to 10 cm, the peak current density is estimated to be no more than two times the average.

The molybdenum optics measurements provide a reference point for the carbon-carbon optics measurements, but signif-

icant differences in geometry prevent a one-to-one comparison. These differences include 1) grid thickness (the carbon-carbon grids are about twice as thick as the molybdenum); 2) grid shape (the carbon-carbon optics are flat, whereas the molybdenum optics are dished); and 3) hole profile (the carbon-carbon is tapered 6 deg due to the laser machining process, whereas the molybdenum is cupped due to the chemical milling process).

Results

Voltage Standoff Capability

With the carbon-carbon grids installed in the grid mount, gapped to 0.58 mm, and exposed to atmospheric conditions, the voltage difference between the grids was slowly increased. Arcing was observed initially as the voltage was increased above 1000 V. By pausing at each occurrence, the rate of arcing decreased and eventually stopped. The voltage was eventually increased to 2500 V. After some initial arcing, the grids were held at 2500 V for several minutes with no further arcing observed. The estimated voltage gradient at 2500 V was 4300 V/mm. Inspection of the grids under a microscope following the test showed that the arcing had no visible effect on the grids, other than to produce some slight, localized, surface discoloration.

The same test was repeated in a vacuum chamber pumped down to about 1×10^{-5} Torr. No arcing was visible up to 3500 V. At 3500 V, a small, steady current of about 0.5 mA was measured. At 3750 V, arcing began, but as before, it subsided with time. Eventually, 5000 V was reached with only occasional arcing, but a steady current of about 1 mA was measured. (A similar current was measured in a subsequent test of a pair of pyrolitic graphite grids, which had smooth, untextured surfaces.) The estimated voltage gradient at 5000 V was 8600 V/mm.

The molybdenum grids were then installed on the grid mount and also gapped to 0.58 mm. In air, the voltage was increased to 2500 V with no arcing observed. At 2500 V, the estimated voltage gradient was 4300 V/mm.

The same test was repeated in a vacuum chamber pumped down to about 1×10^{-5} Torr. No arcing was observed until the voltage reached 5000 V. Then, a few arcs were observed over a period of several minutes. The estimated voltage gradient at 5000 V was 8600 V/mm. No leakage current between the molybdenum grids was detected.

Although voltage breakdown limit measurements were not conducted while the thruster was running, the maximum voltage gradient attained during testing can be reported. For the carbon-carbon grids, an estimated maximum voltage gradient of 6420 V/mm occurred at an average current density of 2.2 mA/cm^2 and a cold grid gap of 0.2 mm. For the molybdenum grids, an estimated maximum voltage gradient of 1840 V/mm occurred at an average current density of 2.2 mA/cm^2 and a cold grid gap of 0.6 mm. The molybdenum grids are capable of higher voltage gradients, but for this test (wherein the molybdenum grids were held at larger grid gaps than the carbon-carbon grids to compensate for differences in thickness), 1840 V/mm was the highest gradient observed.

Maximum Perveance Condition

Figure 3a shows a plot of accelerator grid impingement current as a function of beam voltage for the molybdenum grids at an effective acceleration length of 1.35 mm. Figure 3b shows the same plot for the carbon-carbon grids. Data for the other effective acceleration lengths showed similar trends.

From these plots, the "knee" in the curve was determined, and the voltage at that point was recorded as the minimum beam voltage. The minimum total voltage was then calculated from the minimum beam voltage and the accelerator grid voltage (accelerator grid voltage was fixed for each run and is tabulated in Fig. 3).

The knee in the curve was determined by 1) fitting straight lines to the data on either side of the knee, 2) bisecting the angle formed by the two lines drawn in 1, and then 3) determining where the angle bisector intercepted the recorded data.

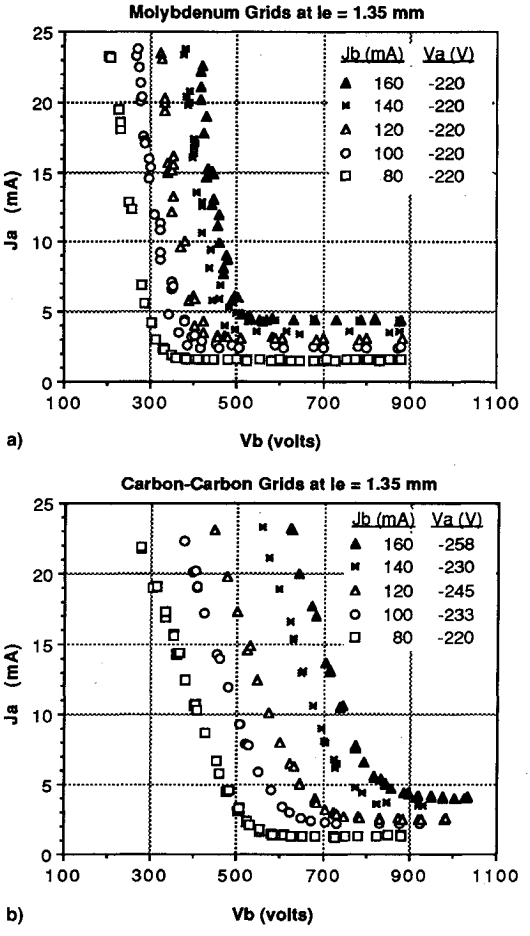

Fig. 3 Accelerator grid impingement current as a function of beam voltage for a) molybdenum grids and b) carbon-carbon grids.

The rapid onset of direct ion impingement for the molybdenum grids (as characterized by the sharp knees in the curves of Fig. 3a) implies all areas of the grid encountered direct impingement at about the same voltage and, hence, that the grids were well aligned. Also, the cupped profile of the holes in the molybdenum grids, which makes a sharp cusp at the point of minimum hole diameter, is believed to contribute to the sharpness of the knees in the curves of Fig. 3a. The more gradual onset of direct impingement for the carbon-carbon grids is a possible symptom of poor grid alignment, but inspection of the carbon-carbon grids before and after testing indicated that the alignment was as good or better than for the molybdenum grids. This characteristic of the carbon-carbon grids is therefore attributed to their thickness. The nonuniform potential in the edge regions of a thick accelerator grid hole produce electric fields directed toward the accelerator hole edge.[8] As the impingement-limited perveance condition is approached, the ion beamlet diameters increase and a greater number of ions are influenced by these edge or fringe fields. This results in a gradual increase in direct impingement on the walls of the accelerator grid holes as beam (and therefore total) voltage is decreased.

Figure 4 is a plot of the fraction of Child's law current vs total voltage for all runs at impingement-limited conditions. The carbon-carbon data show consistent slopes and spacing from one effective acceleration length to another. The molybdenum data, however, have varying slopes and are not consistently spaced. The carbon-carbon data reflect the expected behavior, wherein the spread from curve to curve is due to the change in J_c with effective acceleration length [Eq. (4)], and the positive slopes reflect the fact that the beam current increases with total voltage at a rate somewhat faster

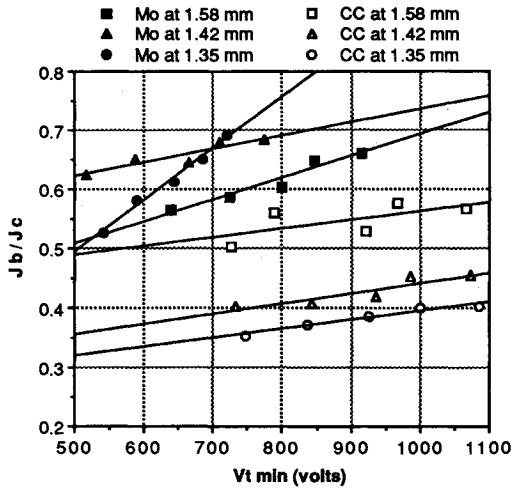

Fig. 4 Impingement-limited beam current.

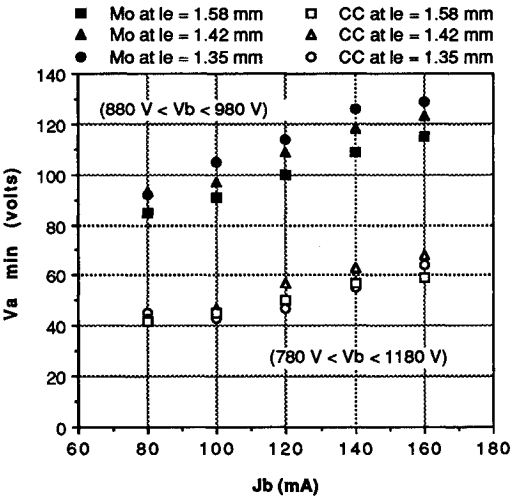

Fig. 5 Electron backstreaming limit.

than is predicted by Child's law.[9] For the molybdenum data, however, the curves are not spread as expected, and the slopes, although positive, are not parallel. The unexpected spread may be due to the uncertainty in measuring the grid gap (and therefore, the effective acceleration length) with the dished molybdenum grids. A cause for the differences in slope has not been determined. In any event, for all cases the molybdenum grids produced a higher fraction of Child's law current than the carbon-carbon grids. This is an expected result given the greater thickness of the carbon-carbon grids.

Electron Backstreaming Limit

Figure 5 shows the electron backstreaming limit for each run. The thicker carbon-carbon accelerator grid provides a more effective shield between the plasma and external electrons than does the molybdenum accelerator grid. Hence, a lower accelerator grid voltage is achieved prior to backstreaming for the carbon-carbon grid than for the molybdenum accelerator grid.

Figure 6 overplots the electron backstreaming data with Kaufman's backstreaming parameter,[10] a correlation given by

$$(1 - R_{\max}) \frac{l_e}{d_a} = \frac{e^{-t_a/d_a}}{2\pi} \tag{6}$$

where $R_{\max}$ is the net-to-total voltage ratio at the onset of electron backstreaming. This correlation includes the effects of grid thickness and does well at predicting the behavior of the carbon-carbon grids.

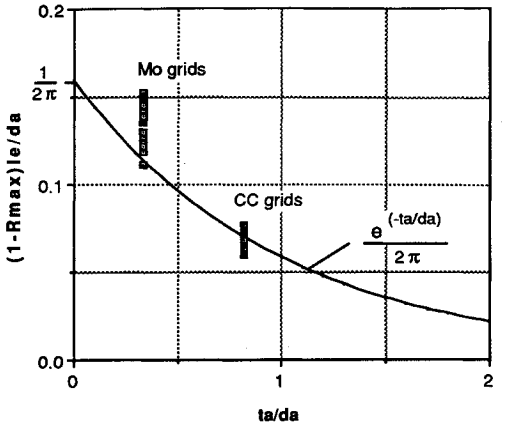

Fig. 6 Kaufman's electron backstreaming parameter.

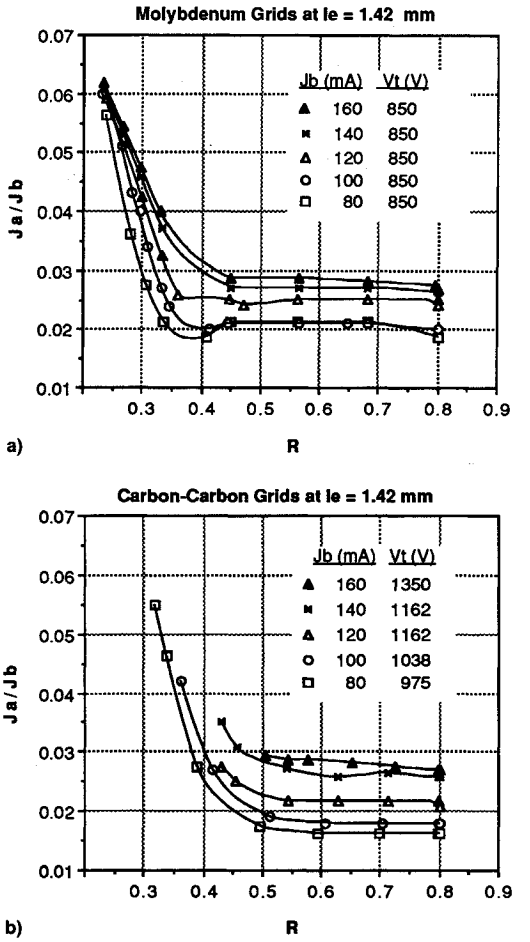

Fig. 7 Variation of accelerator grid impingement current as a function of R for a) molybdenum grids and b) carbon-carbon grids. The knee in the curves is the defocusing limit.

Defocusing Limit

Figures 7a and 7b show the ratio of accelerator grid impingement current to beam current plotted as a function of R for an effective acceleration length of 1.42 mm. Data at other effective acceleration lengths showed similar trends.

For an effective acceleration length of 1.42 mm, the defocusing limit occurred for the molybdenum grids at R values between 0.3–0.4. At the same effective acceleration length, the defocusing limit occurred for the carbon-carbon grids at R values between 0.4–0.5. This difference also may be explained by the difference in grid thickness, where the radial component of the electric field causes earlier defocusing with the thicker carbon-carbon grid.

Conclusions

An experimental investigation to demonstrate the operation of a carbon-carbon ion optics set has been described. As part of the demonstration, selected performance characteristics were evaluated to determine if any unusual or unexpected behavior arose relative to conventional molybdenum optics. The only difference noted that was not accounted for by geometry differences was the observance of a 1-mA leakage current across the carbon-carbon grids when subject to a large (8600 V/mm) voltage gradient in a vacuum. No leakage current was observed with the molybdenum grids under the same conditions. The carbon-carbon grids delivered stable operation at a cold grid gap of 0.2 mm, an average current density of 2.2 mA/cm^2, and an inferred voltage gradient of 6400 V/mm based on the cold grid gap. Differences between the carbon-carbon and molybdenum grid performance characteristics (i.e., maximum perveance condition, electron backstreaming limit, and defocusing limit) were consistent with those expected from the known differences in geometry (primarily grid thickness). The carbon-carbon grids proved to be rugged and showed no visible damage where arcing occurred.

Further testing is required to verify that carbon-carbon grids are substantially more resistant to sputter erosion than molybdenum grids. Once that is established, then efforts can focus on optimizing carbon-carbon grid fabrication through improved manufacturing techniques.

Acknowledgments

The authors would like to thank M. J. Patterson of NASA Lewis Research Center for his help in test matrix development, M. E. Rorabaugh of Boeing for his assistance in materials selection and processing, and D. M. Skene of Boeing for his support in the laboratory.

References

[1]Patterson, M. J., "Low-Isp Derated Ion Thruster Operation," AIAA Paper 92-3203, July 1992.

[2]Wehner, G. K., "The Aspects of Sputtering in Surface Analysis Methods," *Methods of Surface Analysis*, edited by A. W. Czanderna, Elsevier, Amsterdam, The Netherlands, 1975, p. 10.

[3]Kerslake, W. R., and Pawlik, E. V., "Additional Studies of Screen and Accelerator Grids for Electron-Bombardment Ion Thrusters," NASA TN D-1411, Aug. 1963, p. 11.

[4]Monheiser, J. M., and Wilbur, P. J., "An Experimental Study of Impingement-Ion-Production Mechanisms," AIAA Paper 92-3826, July 1992.

[5]Garner, C. E., and Brophy, J. R., "Fabrication and Testing of Carbon-Carbon Grids for Ion Optics," AIAA Paper 92-3149, July 1992.

[6]Jahn, R. G., *Physics of Electric Propulsion*, McGraw-Hill, New York, 1968, Chap. 7.

[7]Patterson, M. J., and Foster, J. E., "Performance and Optimization of a 'Derated' Ion Thruster for Auxiliary Propulsion," AIAA Paper 91-2350, June 1991.

[8]Aston, G., Kaufman, H. R., and Wilbur, P. J., "Ion Beam Divergence Characteristics of Two-Grid Accelerator Systems," *AIAA Journal*, Vol. 16, No. 5, 1978, pp. 516–524.

[9]Rawlin, V. K., "Studies of Dished Accelerator Grids for 30-cm Ion Thrusters," AIAA Paper 73-1086, Oct. 1973.

[10]Kaufman, H. R., "Technology of Electron-Bombardment Ion Thrusters," *Advances in Electronics and Electron Physics*, edited by L. Marton, Vol. 36, Academic Press, New York, 1974.